

Shape coexistence near the neutron number $N=20$: First identification of the $E0$ decay from the deformed 0_2^+ state in ^{30}Mg

W. Schwerdtfeger¹, P.G. Thirolf¹, K. Wimmer¹, D. Habs¹, H. Mach², T.R. Rodriguez⁴,
V. Bildstein³, J.L. Egido⁴, L.M. Fraile⁵, R. Gernhäuser³, R. Hertzenberger¹, K. Heyde⁶,
P. Hoff⁷, H. Hübel⁸, U. Köster⁹, T. Kröll³, R. Krücken³, R. Lutter¹, T. Morgan¹ and P. Ring³

¹Ludwig-Maximilians-Universität München, D-85748 Garching, Germany

²Department of Nuclear and Particle Physics, Uppsala University, SE-75121 Uppsala, Sweden

³Physik Department E12, Technische Universität München, D-85748 Garching, Germany

⁴Universidad Autonoma de Madrid, E-28049 Madrid, Spain

⁵Universidad Complutense, E-28040 Madrid, Spain

⁶Department of Subatomic and Radiation Physics, Universiteit Gent, B-9000, Gent, Belgium

⁷Department of Chemistry, University of Oslo, N-0315 Oslo, Norway

⁸Helmholtz-Institut für Strahlen- und Kernphysik, Universität Bonn, D-53115 Bonn, Germany

⁹Institut Laue-Langevin, F-38000 Grenoble, France

(Dated: October 26, 2018)

The 1789 keV level in ^{30}Mg was identified as the first excited 0^+ state by measuring its $E0$ transition to the ground state. The measured small value of $\rho^2(E0, 0_2^+ \rightarrow 0_1^+) = 5.7(14) \cdot 10^{-3}$ implies a very small mixing of competing configurations with largely different intrinsic quadrupole deformation near $N=20$. Axially symmetric Beyond-Mean-Field configuration mixing calculations identify the ground state of ^{30}Mg to be based on neutron configurations below the $N=20$ shell closure, while the excited 0^+ state mainly consists of a two neutrons excited into the $\nu 1f_{7/2}$ orbital. Using a two-level model, a mixing amplitude of 0.08(4) can be derived.

PACS numbers: 23.40.-s, 23.20.Nx, 23.20.Js, 27.30.+t

One of the most studied phenomena in the region of neutron-rich atomic nuclei around the $N=20$ shell closure is the occurrence of strongly deformed ground states in Ne, Na and Mg isotopes. This so-called 'island of inversion' [1] (discovered already more than 30 years ago [2]) finds its origin in the promotion of a pair of neutrons across the $N=20$ shell gap, thus leading to the intrusion of deformed low-lying ($2p2h$) configurations below the spherical ($0p0h$) states compared to nuclei closer to β stability. Despite considerable efforts the precise localization of the transition from normal to intruder-dominated configurations is not yet finally settled and even the origin of the large collectivity of the $0_{gs}^+ \rightarrow 2_1^+$ transition in ^{32}Mg is still under debate [3]. A coexistence of spherical and deformed 0^+ states is predicted to exist within a small region around $N=20$ in the neutron-rich Mg nuclei [4, 5], the 'island of inversion'. So far studies on spectroscopic properties have focused on $B(E2)$ values between the 0^+ ground state and the first excited 2^+ state [6, 7, 8, 9, 10, 11, 12], however no excited 0^+ state has been experimentally observed in these nuclei. While ^{32}Mg , which is conventionally considered a closed-shell nucleus, exhibits a strongly deformed ground state as indicated by the large value of $B(E2; 0_{gs}^+ \rightarrow 2_1^+) = 454(78)e^2\text{fm}^4$ [6], the ground state of ^{30}Mg is expected to be much less deformed, whereas a (deformed) excited 0_2^+ state is predicted at an energy between 1.7 and 2 MeV [13, 14, 15, 16] that has so far escaped observation.

It is the purpose of this Letter to report the unambiguous identification of the coexisting 0_2^+ state in ^{30}Mg using conversion electron spectroscopy and to discuss the

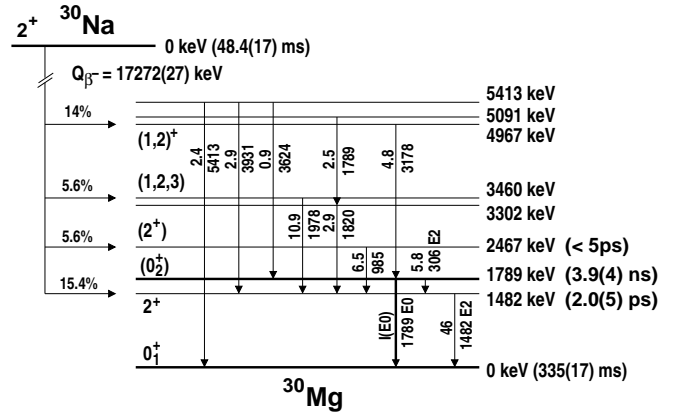


FIG. 1: Low-energy part of the level scheme of ^{30}Mg [17].

configuration mixing between normal and intruder configurations at the border of the 'island of inversion'.

Resulting from fast timing γ -spectroscopy studies [17], the 1789 keV level in ^{30}Mg emerged as a strong candidate for the deformed first excited 0_2^+ state due to its long half-life of 3.9(4) ns and the absence of a ground state γ transition. Fig. 1 displays our present knowledge on the low-energy part of the level scheme of ^{30}Mg [17], triggering our search for the deformed 0_2^+ state in ^{30}Mg via conversion electron spectroscopy following β decay of ^{30}Na at the ISOLDE facility at CERN. The radioactive ^{30}Na atoms [$t_{1/2} = 48.4(17)$ ms] were produced by sending 1.4 GeV protons provided by the CERN PS Booster with an intensity up to $3.2 \cdot 10^{13}$ p/pulse onto a $\text{UC}_x/\text{graphite}$ target (heated to $\sim 2050^\circ\text{C}$). On average every second

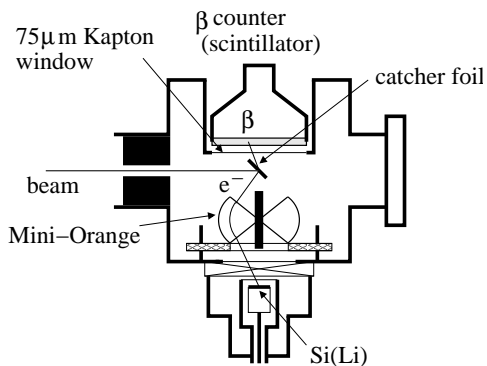


FIG. 2: Sketch of the experimental setup (top view). The Germanium detector that was mounted vertically on top of the target chamber is not shown.

pulse (repetition rate of 1.2 s) was used. The reaction products diffusing out of the target were surface-ionized and the extracted 1^+ ions were mass separated by the ISOLDE High Resolution Separator at a kinetic energy of 40 keV. This $A = 30$ beam was sent to the experimental setup which is illustrated in Fig. 2. The beam was stopped in the center of the target chamber in a 0.1 mm thick Al foil to examine the β decay of ^{30}Na to excited states of ^{30}Mg . In order to detect the E0 decay electrons with high resolution (3.0 keV FWHM) a liquid nitrogen cooled Si(Li) detector with an active surface of 500 mm² and a thickness of 5 mm was used. The detector was operated in conjunction with a Mini-Orange [18] consisting of 8 wedge-shaped ($\text{Nd}_2\text{Fe}_{14}\text{B}$) permanent magnets creating a toroidal magnetic field ($B \sim 160$ mT) arranged around a central Pb absorber (diameter: 16 mm, length: 50 mm) in order to block γ rays from the catcher foil. Towards the catcher foil the absorber was covered by a Cu cap in order to suppress X-ray production. The transmission efficiency of the spectrometer was 3.2 % around 1.7 MeV, optimized for the expected E0 transition in ^{30}Mg . A 0.2 mm thick plastic scintillator (BC-404, diameter 50 mm) read out by a 2" photomultiplier tube was mounted at a distance of 13 mm to the target, resulting in a solid angle coverage of $\Omega/4\pi = 21$ %. This detector served as trigger on β -decay electrons and was operated in coincidence with the Mini-Orange spectrometer. In order to identify the beam composition and for normalisation purposes γ rays following the β decay were detected using a Ge detector mounted on top of the target chamber.

In order to achieve optimum sensitivity for the expected weak E0 transition, the setup was optimized for the reduction of the potentially dominant coincident background from Compton electrons in view of the large Q value of the ^{30}Na β decay (17272(27) keV). Consequently the Al target chamber was coated at the inside by 15 mm thick Teflon plates in order to absorb Compton-scattered electrons. The germanium detector served as monitor of the $A = 30$ beam composition, which turned out to consist almost entirely of ^{30}Na at a total intensity

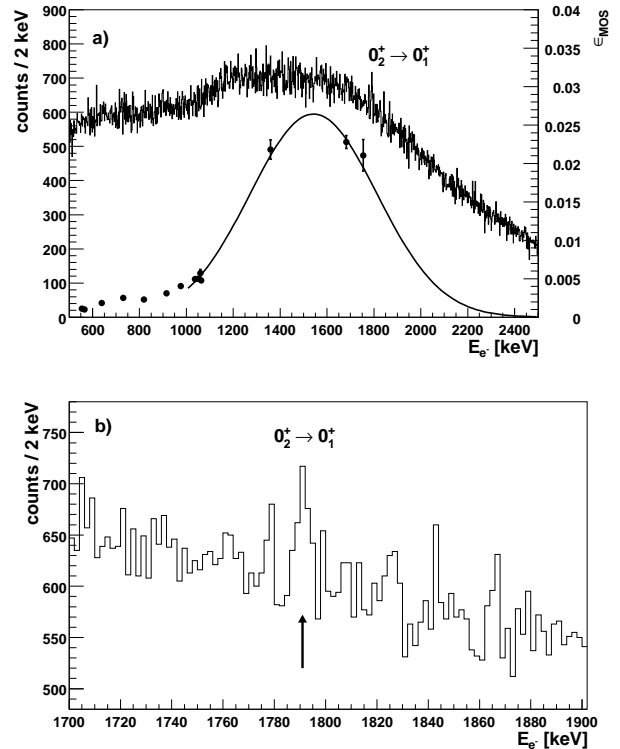


FIG. 3: a) Background-subtracted electron spectrum measured in coincidence with signals in the plastic detector, gated on time differences ≤ 500 ms between the proton pulse and the registered β decay signal. Also shown is the transmission efficiency curve of the Mini Orange spectrometer. The rapidly increasing β decay energy spectrum ($Q_\beta = 17.3$ MeV) gives rise to the rather high background remaining below the transmission maximum. b) Expanded view to the electron spectrum in the region of the E0 transition in ^{30}Mg .

of 4100 decays/second. Since the half-life of ^{30}Na decay is much shorter compared to ^{30}Mg or ^{30}Al originating from the β decay chain, during the analysis events with short lifetimes (≤ 400 ms) were selected from a decay time measurement relative to the initial proton pulse, thus enhancing spectral contributions from ^{30}Na .

The resulting electron spectrum detected with the Si(Li) detector in coincidence with β -decay electrons is shown in Fig. 3. The upper panel a) displays the spectrum over a wide energy range, together with the transmission efficiency curve of the Mini-Orange spectrometer (solid line). The rather high yield below the transmission maximum results from the rapidly increasing β decay energy spectrum. In Fig. 3b) the sought $0_2^+ \rightarrow 0_1^+$ E0 transition at 1788 keV is visible. 304(60) counts were detected in the peak during 143 hrs of beamtime (MO transmission efficiency: 2.0(2)%). With an energy resolution of 3.0 keV for the Si(Li) detector spanning K and L conversion in ^{30}Mg ($E_K = 1.3$ keV), the monopole strength $\rho^2(\text{E0})$ can be determined by the ratio of E0 (K+L) conversion intensity to the E2 γ intensity and the

	$E_x(2_1^+)$ (MeV)	$E_x(0_2^+)$ (MeV)	$B(E2, 0_1^+ \rightarrow 2_1^+)$ ($e^2 fm^4$)	$\rho^2(E0) \cdot 10^3$
Theory	2.03	2.11	334.6	46
Experiment	1.482	1.789	241(31) [10]	5.7(14)

TABLE I: Results from Beyond Mean Field calculations with Gogny force for ^{30}Mg compared to experimental values.

γ lifetime τ_γ of the 0_2^+ state as [19]

$$\rho^2(E0) = \frac{I_{K+L}(E0)}{I_\gamma(E2)} \cdot \frac{1}{\Omega_{K+L}(E0)} \cdot \frac{1}{\tau_\gamma}. \quad (1)$$

The γ intensity of the E2 transition at 306 keV measured within the β - γ coincidence condition using the Ge detector is $I_\gamma(E2) = 6.591 \cdot 10^4$ ($\epsilon_\gamma = 0.0019$), the half-life $T_{1/2}$ of the 0_2^+ state was measured to be 3.9(4) ns [17] (corresponding in our case to $\tau_\gamma \approx \tau = 5.6(6)$ ns) and the electronic Ω factor is $\Omega_{K+L} = 1.39 \cdot 10^7/\text{s}$ [20]. This finally allows to derive the electric monopole matrix element $\rho^2(E0, ^{30}\text{Mg}) = 5.7(14) \cdot 10^{-3}$, which corresponds to an intensity of the E0 transition of $I = 2.2(5) \cdot 10^{-5}$ and a partial E0 lifetime of $\tau(E0) = 1.26(31) \mu\text{s}$.

In the 'island of inversion' the deformed configuration based on two neutrons being excited from the $\nu 1d_{3/2}$ to the intruder orbital $\nu 1f_{7/2}$ keeps pace with the normal spherical one as illustrated by the case of ^{32}Mg , where the intruder state even becomes the ground state. In such a situation of competing configurations and in the absence of mixing one expects either a deformed 0_1^+ and a nearly spherical 0_2^+ state or the other way around. Since the E0 operator is a *single particle* one, one expects in both cases small values of the monopole matrix element $M(E0) \equiv \langle 0_g^+ | T(E0) | 0_{\text{exc}}^+ \rangle$ with $T(E0)$ being the E0 operator as given by Wood et al. [21] and $\rho^2(E0) \equiv |M(E0)/eR^2|^2$ with the nuclear radius $R = 1.2 A^{1/3}$ fm. Inducing configuration mixing, somewhat larger values of $\rho^2(E0)$ can be expected. In ^{30}Mg the small experimental value of $\rho^2(E0) = 5.7(14) \cdot 10^{-3}$ points towards the presence of small mixing. However, an important question that remains to be answered concerns the nature of the two 0^+ states and the amount of mixing of the $\nu 1d_{3/2}$ and $\nu 1f_{7/2}$ configurations. Concerning the 0_1^+ state there are strong experimental [8, 10] and theoretical [13, 14, 16] indications that in ^{30}Mg the inversion has not taken place.

In order to understand the experimental findings calculations going beyond the mean-field by incorporating configuration mixing [22] have been performed using the finite range density dependent Gogny force with the D1S parameterization [23]. The results of these calculations for ^{30}Mg are listed and compared to experimental values in Table I. The excitation energy of the 0_2^+ state and the $B(E2; 0_1^+ \rightarrow 2_1^+)$ value agree reasonably well with the experimental values, while the value of $\rho^2(E0)$ overestimates the experimental result.

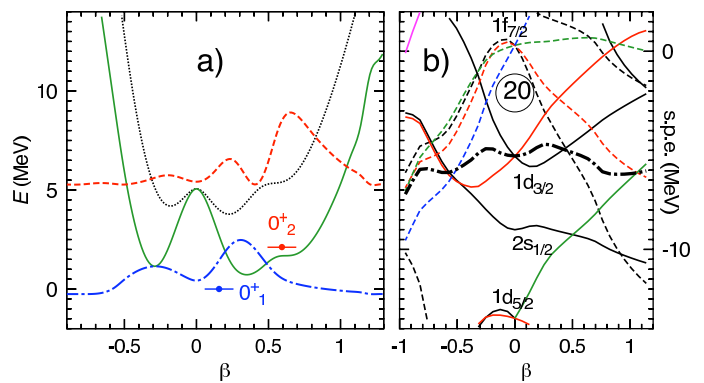


FIG. 4: Theoretical results for ^{30}Mg : a) The dotted line corresponds to results of particle number projected (PNP) calculations, the green full line to the $J = 0$ energy surface and the blue (red) dashed-dotted (dashed) line represents the collective wave function of the 0_1^+ (0_2^+) state. b) Neutron single-particle energies as a function of deformation. The thick dash-dotted line represents the Fermi level (color).

In Fig. 4a, the particle number projected (PNP) potential energy curve displays both a mild prolate and an oblate minimum at small deformation and a shoulder at larger β values. Inspecting the neutron single-particle energies in the right hand panel, we see that the two minima at moderate deformation correspond to the two minima of the single-particle energies of the $\nu 1d_{3/2}$ orbitals just below the Fermi level (notice that this is not the case in ^{32}Mg , see [13]), while the shoulder appears at deformations at which two neutrons already occupy the $\nu 1f_{7/2}$ orbital. The angular momentum projection provides an additional energy lowering with respect to the PNP energy (the full line in panel (a)), and finally configuration mixing leads to the 0_1^+ and 0_2^+ states positioned in the E- β plane (Fig. 4a) according to their energy and average deformation. The composition of the collective wave functions of these two states, i.e. the weights of the corresponding β values being admixed, indicates the character of the state. We notice that the 0_1^+ state (blue dotted-dashed line) is a mixture of prolate and oblate $\nu 1d_{3/2}$ configurations which average to a small intrinsic deformation of $\beta = 0.16$. The 0_2^+ state (blue dashed line), on the other hand, is a well deformed state with $\beta = 0.59$ consisting to a large part of a $\nu 1f_{7/2}$ configuration with very small admixtures of the $\nu 2d_{3/2}$ configuration. These results are consistent with the experimental finding of a very small matrix element connecting both 0^+ levels.

It is known [24, 25] that the calculation of $\rho^2(E0)$ is very sensitive to small variations of the interaction matrix elements and in particular to small admixtures of different shapes. Ideally, one needs to consider triaxial shapes in the calculations. Due to the complexity of a fully triaxial angular momentum projected calculation, at present, we had to impose restrictions to axial symmetric states only. Neglecting triaxial effects might be a worse approximation in the calculation of $\rho^2(E0)$ than

in the case of other observables like energies or B(E2) strengths, because in the latter cases the intrinsic state of the initial and final wave functions is the same, while in the case of $\rho^2(E0)$ these states, in general, have a rather different dependence on γ . So there is room for possible improvement over the present theoretical $\rho^2(E0)$ value.

In order to quantify the mixing amplitude between the deformed and spherical configurations, we have also analyzed our experimental results making use of a phenomenological two-level mixing model. Here the monopole matrix element strongly depends on the mixing amplitude a between the two intrinsic (spherical and deformed) 0^+ states, i.e.

$$\begin{aligned} |0_g^+\rangle &= \sqrt{1-a^2}|0_{\text{sph}}^+\rangle + a|0_{\text{def}}^+\rangle, \\ |0_{\text{exc}}^+\rangle &= -a|0_{\text{sph}}^+\rangle + \sqrt{1-a^2}|0_{\text{def}}^+\rangle. \end{aligned} \quad (2)$$

Within the quadrupole deformed rigid rotor model the strength of the E0 transition can be described as [21]

$$\rho^2(E0) = \left(\frac{3}{4\pi}Z\right)^2 \cdot a^2 \cdot (1-a^2) \cdot (\beta_1^2 - \beta_2^2)^2, \quad (3)$$

with β_1, β_2 the equilibrium quadrupole deformations corresponding to the $|0_{\text{sph}}^+\rangle$ and $|0_{\text{def}}^+\rangle$ intrinsic configurations, respectively. Using the deformation values of the two 0^+ states as calculated above ($\beta_1(0_1^+) = 0.16$, $\beta_2(0_2^+) = 0.59$) together with the experimental value of $\rho^2(E0)$, a value of $a^2 = 0.0067(16)$ can be extracted, resulting in a value of $a = 0.08(4)$ for the mixing amplitude between the two intrinsic 0^+ states. It should be noted that an identical value of $\beta_2(0_2^+) = 0.59$ can be inferred from the phenomenological Grodzins systematics [26], which empirically correlates the B(E2; $0_1^+ \rightarrow 2_1^+$) value and the excitation energy of the first excited 2^+ state (here based on the assignment of the 2467 keV level

as being the rotational 2_2^+ state). For ^{30}Mg and ^{32}Mg the B(E2) values predicted by the Grodzins systematics ($256(45) \text{ e}^2\text{fm}^4$ and $410(73) \text{ e}^2\text{fm}^4$) agree remarkably well with the experimental values ($241(31) \text{ e}^2\text{fm}^4$ [10] and $454(78) \text{ e}^2\text{fm}^4$ [6]). This also points to rather pure 0^+ and 2^+ states in the two potential minima, because otherwise deviations from the Grodzins systematics could be expected.

To conclude, conversion electron measurements at ISOLDE have identified the 1789 keV level as the 0_2^+ state in ^{30}Mg . The conversion electrons were measured in coincidence with β decay electrons using a Mini-Orange spectrometer. The monopole strength extracted from measuring the $0_2^+ \rightarrow 0_1^+$ E0 transition is $\rho^2(\text{E0}, ^{30}\text{Mg}) = 5.7(14) \cdot 10^{-3}$, which corresponds to an intensity of the E0 transition of $I = 2.2(5) \cdot 10^{-5}$ and a partial E0 lifetime of $\tau(E0) = 1.26(31) \mu\text{s}$. The small value of the monopole strength indicates a weak mixing and allows for the first time to deduce the mixing amplitude between shape-coexisting 0^+ states near the 'island of inversion' as $a = 0.08(4)$. State of the art beyond-mean-field calculations identify the ground state as based on a mixture of prolate and oblate $\nu 1d_{3/2}$ orbitals and the excited 0_2^+ state on a rather pure $\nu 1f_{7/2}$ level, thereby confirming a sharp borderline of the 'island of inversion' and a very weak mixing between the competing configurations.

Acknowledgments

This work was supported by BMBF (contracts 06ML234, 06MT238 and 06BN109), by the European Commission within FP6 through I3-EURONS (contract no. RIDS-CT-2004-506065), by the Swedish Research Council, by MEC (FPA2007-66069) and by the Spanish Consolider-Ingenio 2010 Program CPAN (CSD2007-00042).

-
- [1] E.K. Warburton et al., Phys. Rev. **C 41** (1990) 1147.
[2] C. Thibault et al., Phys. Rev. **C 12** (1975) 644.
[3] M. Yamagami et al., Phys. Rev. **C 69** (2004) 034301.
[4] K. Heyde and J.L. Wood, J. Phys. **G17** (1991) 135.
[5] J.L. Wood et al., Phys. Rep. **215** (1992) 101.
[6] T. Motobayashi et al., Phys. Lett. **B346** (1995) 9.
[7] H. Iwasaki et al., Phys. Lett. **B 522** (2001) 227.
[8] B. Pritychenko et al., Phys. Lett. **B 461** (1999) 322.
[9] V. Chisté et al., Phys. Lett. **B 514** (2001) 233.
[10] O. Niedermaier et al., Phys. Rev. Lett. **94** (2005) 172501.
[11] O. Niedermaier, Ph.D. thesis, Univ. Heidelberg (2005), <http://deposit.ddb.de/cgi-bin/dokserv?idn=975806416>.
[12] A. Gade et al., Phys. Rev. Lett. **99** (2007) 072502.
[13] R. Rodríguez-Guzmán, J.L. Egido, L.M. Robledo, Nucl. Phys. **A709** (2002) 201.
[14] E. Caurier et al., Nucl. Phys. **A693** (2001) 374.
[15] F. Nowacki et al., priv. communic. in: D. Guillemaud-Mueller et al., Eur. Phys. Journ. **A13** (2002) 63.
[16] T. Otsuka, Eur. Phys. Journ. **A20** (2004) 69.
[17] H. Mach et al., Eur. Phys. J. **A25** (2005) s01 105.
[18] J. van Klinken and K. Wisshak, Nucl. Instr. Meth. **98** (1972) 1; J. van Klinken, S.J. Feenstra, K. Wisshak and H. Faust, Nucl. Instr. Meth. **130** (1975) 427; J. van Klinken, S.J. Fenstra and G. Dumond, Nucl. Instr. Meth. **151** (1978) 433.
[19] T. Kibédi and R. H. Spear, Atomic Data and Nuclear Data Tables, **89** (2005) 77.
[20] J. Kantele, Handbook of Nuclear Spectroscopy, Academic Press 1995, ISBN 0-12-396440-7.
[21] J.L. Wood et al., Nucl. Phys. **A651** (1999) 323.
[22] T.R. Rodríguez, J.L. Egido, Phys. Rev. Lett. **99** (2007) 062501.
[23] J.F. Berger, M. Girod, D. Gogny, Nucl. Phys. **A 428** (1984) 23c.
[24] E. Bouchez et al., Phys. Rev. Lett. **90** (2003) 082502.
[25] A. Petrovici et al., Nucl. Phys. **A665** (2000) 333.

- [26] S. Raman, C.W. Nestor, P. Tikkanen, *At. Data Nucl. Data Tab.* 78 (2001) 1.